Supporting Information

Facet Dependent Islet Amyloid Polypeptide (IAPP) Interactions with Gold Nanoparticles: Implications for Fibril Formation and Peptide-Induced Lipid Membrane Disruption

Shih-Ting Wang[1, 2], Yiyang Lin[1, 2], Nevena Todorova[3], Yingqi Xu[4], Manuel Mazo[1, 2], Subinoy Rana[1, 2], Vincent Leonardo[1, 2], Nadav Amdursky[1, 2], Christopher D. Spicer[1, 2], Bruce D. Alexander[5], Alison A. Edwards[6], Steve J. Matthews[4], Irene Yarovsky[3], and Molly M. Stevens[1, 2*]

[1]Department of Materials, Imperial College London, London, SW7 2AZ, UK
[2]Department of Bioengineering and Institute of Biomedical Engineering, Imperial College London, London, SW7 2AZ, UK
[3]School of Engineering, RMIT University, GPO Box 2476, Melbourne, Victoria 3001, Australia
[4]Department of Life Sciences, Imperial College London, London, SW7 2AZ, UK
[5]Department of Pharmaceutical, Chemical and Environmental Science, University of Greenwich, Central Avenue, Chatham, Kent, ME4 4TB, UK
[6]Medway School of Pharmacy, Universities of Kent and Greenwich at Medway, Central Avenue, Chatham, Kent, ME4 4TB, UK

Corresponding author:
*Email: m.stevens@imperial.ac.uk

Materials

Full-length islet amyloid polypeptide (IAPP-amide, 95 %) was purchased from Cambridge Bioscience, and IAPP 20-29 was synthesised by solid phase peptide synthesis using the typical Fmoc chemistry. Gold nanoparticles (AuNPs) were purchased from BBI Solutions, and all other chemicals were obtained from Sigma-Aldrich (U.K.).

Preparation of IAPP stock solution. To remove pre-existing IAPP aggregates, the full-length IAPP powder was dissolved in hexafluoro-2-propanol (HFIP), and kept in a sealed vial for 8 h at room temperature. After evaporating the solvent, the treated

IAPP powder was stored at -20 °C. For IAPP 20-29, the stock solution was prepared at a concentration of 10 mM in dimethyl sulfoxide (DMSO) and stored at -20 °C.

Diffusion-ordered NMR spectroscopy (DOSY-NMR). For high-resolution DOSY ^{1}H NMR (Bruker NMR 600) analysis, IAPP (50 μM) was dissolved in D_2O with or without 2 nm AuNPs (BBI, 62 nM) and loaded into standard 5-mm tubes before NMR measurement. The gradient pulses were adjusted to 1.4 ms, and 2.2 ms for IAPP without and with 2 nm AuNPs, respectively. The spectra width was 15000 Hz, and the free induction decay contained 8192 data points. For all of the experiments, the **ledbpgppr2s1d** pulse sequence was used, and 10 spectra of 128 transients each were collected with gradient pulse amplitudes ranging from 0.5 to 45 $G \cdot cm^{-1}$, where ~ 90-95 % decrease was achieved at the largest gradient amplitudes. The baselines of all arrayed spectra were corrected before processing the data. After data acquisition, each free induction decay was apodised with Gaussian window multiplication at LB = -14 Hz and GB = 0.06 Hz, and Fourier-transformed. The spectra acquired with the lowest gradient was used to obtain the relative intensities in the region between 1.25 and 0.70 ppm. The diffusion coefficient was calculated by fitting the experimental data to the Stejskal-Tanner formula[1]:

$$S(Gz) = S(0)*\exp[-D\gamma\ 2\delta 2(Gz)2(\Delta-\delta/3)]FFS15$$

where $S(G_z)$ and $S(0)$ are the signal intensities obtained with respective gradients strengths of G_z and 0, D is the diffusion coefficient, γ is the gyromagnetic constant, δ is the gradient pulse duration, and Δ is the diffusion delay.

Gel electrophoresis. Agarose gel (0.5 wt%) was prepared in Tris/Borate/EDTA (TBE, 1X) buffer with 25 wells, and 1.0 mm in thickness. IAPP-AuNPs samples were prepared by incubating 5 μL of IAPP monomers at different concentrations (8, 4, 2, 0.4, 0.2, 0.04, and 0.02 μM in deionised water) with 15 μL of 5 nm AuNPs (62 nM) for 1 h. After mixing with 1 μL of glycerol, 20 μL of the IAPP-AuNP solutions were loaded into each well. The gel was run at 120 V for 5-10 min before imaging under white light.

Carr-Purcell-Meiboom-Grill (CPMG) NMR measurement of proton relaxation. Proton T2 constants were measured from a series of 1d spectra with 0 ms, 8 ms, 16 ms, 24 ms, 32 ms CPMG relaxation, for IAPP in the absence or presence of AuNPs on a 600 MHz Bruker NMR spectrometer, equipped with a triple-resonance z-gradient cryogenic probe optimized for ^{1}H-detection. Data was processed using TOPSPIN 3.1, and the resonance peaks were assigned according to previous reports.[2, 3]

Characterisation of the surface charge of IAPP and AuNPs. The ζ-potential (zeta sizer nanoseries, ZEN3600, Malvern Instruments Ltd.) was obtained with an equilibrium time of 60 s, and the result was the average from three individual measurements. Prior to the measurements, IAPP monomers and fibrils were prepared at 25 μM in 20 mM phosphate buffer (pH 7.5). IAPP fibrils (50 μM) were pre-formed by aging at r.t. in phosphate buffer for 30 h. The AuNP solutions (2 nm, 5 nm, and 10 nm) were diluted by 1:1 (v/v) with buffer before ζ-potential measurement.

IAPP monomers and fibrils induced AuNP aggregation. IAPP monomers and fibrils were diluted to different concentrations (0.1-50 μM) in deionised water. The fibrils were aged at the concentration of 25 μM in 20 mM phosphate buffer (pH 7.5) for 24 h. The assay was prepared in a 96-well plate, with a total volume of 100 μL. Briefly, 20 μL of the peptide solutions was mixed with 60 μL of 33 mM phosphate buffer (pH 7.5). After that, 20 μL of AuNPs (5 nm, 10 nm, and 20 nm) were added to each well before UV-vis measurement. The final concentration of 5 nm, 10 nm, and 20 nm AuNPs are 16.6 nM, 1.89 nM, and 0.23 nM, respectively. The absorption spectra were obtained by the Perkin Elmer EnSpire plate reader, with the wavelength ranging from 450 nm to 850 nm, and intervals of 5 nm.

Isothermal titration calorimetry (ITC). The binding affinity of IAPP to AuNPs was measured by MicroCal iTC_{200} (Malvern Instruments). Typically, 50 μL of freshly prepared IAPP solution prepared at a concentration of 120 μM in deionised water was filled to the syringe, and 180 μL of 5 nm AuNPs (~10.4 nM) was loaded into the sample cell. The titration of AuNPs into IAPP solution was performed every 3 min for 20 injections. The volume of each injection was 2 μL with the exception of the initial delay to be 0.5 μL. The reference power was set at 5 μcal/s and a stirring speed of 750 rpm. The MicroCal Analysis software was used for data analysis. Control experiments were performed by titrating deionised water into the 5 nm AuNP solution (~10.4 nM) in the sample cell, and the measurement methods were the same as for IAPP-AuNP binding experiments. Results in Figure 1, S4, and S5 were presented with the control data subtracted from the original data of IAPP-AuNP binding experiments.

Transmission electron microscopy (TEM) imaging. All imaging was performed with JEOL 2100F TEM, with an acceleration voltage of 200 kV. For sample preparation, 10 μL of the aging solution at different time points were dropped on the 200 mesh copper grid covered with a carbon-stabilised Formvar film. The residual solution was removed after 5 min, and then the sample was negatively stained by 5 μL

of 1 wt% uranyl acetate solution on the grid for 5 min. Elemental analysis was performed by energy dispersive x-ray spectroscopy (EDS) at the dark-field scanning TEM (DF-TEM) mode on the TEM.

Atomic force microscopy (AFM) imaging. AFM imaging was performed on an AFM 5500 Microscope (Keysight technologies, previously Agilent) in tapping mode in air. A HQ:NSC15/Al BS tip (μmasch) was used for the topography imaging (tip radius of 8 nm, resonance frequency of 325 kHz, force constant of 40 N m^{-1}).

Templated growth of AuNPs on IAPP fibrils. Typically, IAPP fibrils were pre-formed by incubating IAPP (100 μM) in 20 mM phosphate buffer (pH 7.5) for 19 h. To this solution, the desired amount of chloroauric acid ($HAuCl_4$) solution was added and the mixture was incubated for 30 min before the addition of 4-(2-hydroxyethyl)piperazine-1-ethanesulfonic acid (HEPES). The mixture was left overnight at r.t. The final concentration of $HAuCl_4$, IAPP and HEPES was 100 μM, 2 μM, and 0.1 M, respectively. The corresponding TEM sample was prepared according to the method discussed above and imaged at an acceleration voltage of 200 kV.

Molecular Dynamics (MD) Simulations. Solvent all-atom MD simulations were used to study the mechanisms of interaction, and dynamics of monomeric and fibrillar IAPP on citrate-coated Au(111) and Au(100) surfaces, which are the most stable and commonly featured facets on AuNPs.[4] The citrate concentration on each surface was based on the ζ-potential determined experimentally (Table 1), and determined using the approach of Brancolini and colleagues.[5] Using the Poisson-Boltzmann formulation, a ζ-potential of -21.4 mV would require a surface charge density of approximately -0.12 *e*/nm^2. A citrate concentration of ~2.7×10^{-10} mol/cm^2 was used for the Au(111) and Au(100) surfaces, and resulted in an equal distribution of citrate molecules and surface charge density of <0.2 *e*/nm^2. The citrate concentration of 1.4-5×10^{-10} mol/cm^2 on AuNPs was within the experimentally determined citrate concentration range.[6, 7] Note that the amorphous character of the citrate adlayer on citrate-capped AuNPs at pH 7 in our simulation was consistent with the result from Lin et al.,[6] in which the adsorption of citric acid on Au(111) electrode was carried at pH 1. Some of the resulting discrepancies in citrate-Au geometries could be accounted for the lack of counterion-mediated stabilisation in the latter system.[8] The monomeric hIAPP structure was taken from the PDB databank (PDB ID 2L86), as shown in Figure S10a.[9] The pre-formed fibril tetramer of IAPP was based on the proposed IAPP fibril

model by Wiltzius et al.,[10] and built in the CreateFibril database, as shown in Figure S10b.[11]

All-atom classical MD simulations were performed using the Gromacs 4.5.6 software package.[12] The intermolecular interactions between IAPP and the citrate-coated Au surfaces were modelled using the GolP-CHARMM force field,[13, 14] which included the dynamic polarization of Au atoms and the modified TIP3P water model.[15] The method using an empirical model of rigid rods, has been shown to be not only computationally efficient by allowing to incorporate the image charge effect in planar interfacial metal force field,[16-18] but also physically realistic.[16] It is worth to note that based on the similar force field developments philosophy between GolP-OPLS[16] and GolP-CHARMM,[13, 14] we consider the citrate parameters used in this study to be consistent with previous studies by Brancolini et al.[5] In all simulations, the Au surfaces were neutral, the geometry of the Au atoms was fixed, but the Au dipole charges were free to move. The simulation unit-cell was 8.79 nm × 10.10 nm and 9.38 × 9.38 nm for the Au(111) and Au(100) facets, respectively. The height of the unit-cell varied between the systems (described below), and the periodic boundary conditions minimum-image convention was never breached. To ensure overall neutral system sodium counterions were incorporated in the simulation unit-cell. Initially, the citrate layer was allowed to relax on each surface for 5 ns of simulations in explicit solvent. The citrate layer exhibited a disordered 3-D morphology with the anions (carboxylate groups) closest to the surface, and were exposed to the solvent, which was in agreement with previous work by Wright and colleagues.[8] The IAPP monomer was then placed ~9 Å from the Au surface and the system was re-solvated. To eliminate any potential bias from the starting orientation, four different initial structures were examined. Starting with the N-terminus closest to the surface, IAPP was rotated 90° by its principal y-axis each time. The same procedure was also applied for the tetramer simulations. It should be noted that the two cysteine residues (C2 and C7) of IAPP are bound by a disulphide bond, and this bond is present in both in its monomeric and fibrillar form. As such the disulphide-bonded cysteine residues cannot participate in the formation of thiol-Au bonds in the MD simulations, although they are able to interact with the Au surfaces experimentally.[19] It should also be noted that in the IAPP fibril model, the disulphide bond is shielded by the N-terminal loop, which makes it sufficiently distant and protected from the Au surface.

In all simulations, periodic boundary conditions were applied with switch cutoffs to calculate the Coulomb, and van der Waals interaction at 1.0 nm. Long-range electrostatics were also calculated using the particle mesh Ewald method (grid spacing of 0.1 nm).[20] MD was performed in the canonical NVT ensemble (constant number of atoms, volume, and temperature) using the Nosé-Hoover thermostat at 300 K.[21] An integration time-step of 2 fs was applied with all bond lengths constrained using the LINCS algorithm.[22] The steepest descent algorithm was applied to minimize the energy in each system, with a convergence criterion of 20 kJ mol^{-1} nm^{-1}. A 500 ps solvent equilibration was performed where IAPP and the citrate molecules were restrained to their starting positions. Each IAPP-citrate-Au system was then allowed to evolve for 100 ns of MD, and equilibration was verified by monitoring the energy and RMSD drifts. Four independent simulations were performed for the monomeric and fibrillar IAPP on Au(111) and Au(100) surfaces, respectively. A total of 1.6 μs of simulation data was collected. The last 50 ns of each simulation were used for statistical analysis. Secondary structure analysis was performed using the STRIDE algorithm in VMD,[23] to identify the conformational preference of monomeric and fibrillar IAPP when adsorbed to each surface. The contact stabilities of individual residues with the Au surface and citrate layer were investigated individually. A contact was defined when any residue atom was within 4 Å of any Au or citrate atom. The residues were grouped based on the conformational domain they were found in (Figure S10), and averaged in order to identify the persistent peptide regions interacting with surface and/or the citrate layer. The water and citrate density were also analysed to determine the role of water/citrate structure on the binding interactions of IAPP to Au surface.

Thioflavin T (ThT) fluorescence assay. ThT assay was performed in a 384-well plate with a total volume of 80 μL. The IAPP solution was prepared at concentrations of 250, 200, 150, 100, 50 μM in phosphate buffer (20 mM, pH 7.5). Then, 8 μL of ThT stock solution (100 μM) was added to the peptide solution. Fluorescence kinetics was measured with Perkin Elmer EnSpire plate reader, with a time interval of 2 min. The excitation wavelength of ThT fluorescence at 440 nm, and the emission wavelength at 485 nm.

Circular dichroism (CD). The kinetic change of secondary structure during IAPP (25 μM) fibrillation was recorded using a Jasco-715 circular dichroism spectrophotometer. The samples were loaded into a rectangular quartz cell with the

light path length of 1 mm. The measurements were performed at a scanning speed of 50 nm/min, data pitch of 0.1 nm, response time of 4 s, and a band width of 2 nm. In Figure 4, the CD kinetics acquired for IAPP-AuNP samples were performed by mixing IAPP (25 μM) with AuNPs at 20.8 nM for 2 nm and 5 nm AuNPs, and 2.1 nM for 10 nm AuNPs. For all the kinetic experiments, there was approximately a 20 min delay from the addition of NPs until the start of the t = 0 scans. Spectral fitting was performed using the software on Dichroweb, including K2D, SELCON3, CONTIN and CDSSTR. However, significant errors were observed for the samples in the presence of AuNPs. The CDSSTR method showed the closest fitting, but a decrease in the β-sheet content after 11 hrs in the presence of 5 nm AuNPs, which was incorrect based on the fibril formation observed from the TEM imaging in Figure 2j-l. It could be that the presence of AuNPs affects the spectral fitting and therefore it was difficult to deconvolute the CD spectra due to the inadequate reference spectra.

Dye leakage assay. The carboxyfluorescein (CF)-encapsulated liposomes were prepared by typical hydration method. Briefly, a mixture of 1-palmitoyl-2-oleoyl-*sn*-glycero-3-phosphocholine (POPC, 2.5 mg), and 1-palmitoyl-2-oleoyl-*sn*-glycero-3-phospho-(1'-*rac*-glycerol) (POPG, 2.5 mg) was dissolved in 1 mL chloroform/methanol. The solvent was evaporated gently by blowing with nitrogen gas for 10 min. Then, the dried lipid films were hydrated with 1 mL, 50 mM of CF in 20 mM, pH 7.5 phosphate buffer, followed by vortexing for 1 min to produce the POPC/POPG (50:50) liposomes. To form narrowly distributed vesicles, the solution was extruded through a 200 nm pore-sized polycarbonate membrane 21 times, and purified by gel filtration with Sephadex G-100 column eluted with the buffer (in 20 mM, pH 7.5 phosphate).

To perform the dye leakage test, IAPP solution (12.5 μM) was prepared in the phosphate buffer (20 mM, pH 7.5) immediately before diluting into the CF-encapsulated liposome/AuNP solution with 5 nm AuNPs at different concentrations (84, 42, 21, 10, 0 nM). The final concentrations of IAPP and liposomes were 0.31 μM and 12.5 μg/mL, respectively. For IAPP fibril-induced dye leakage, the IAPP solution (25 μM) was left undisturbed for 4 hrs, followed by mixing with different concentrations of 5 nm AuNPs (42, 21, 10, 0 nM) for 10 min, and the addition of CF-encapsulated liposomes. The final concentrations of IAPP and liposomes were 1 μM and 0.3 mg/mL, respectively. Fluorescence intensity was measured with the excitation wavelength of 485 nm, and the emission wavelength of 520 nm. Triton-X (0.25 wt%)

was added to break the liposomes and the dye leakage of each sample was calculated by setting the fluorescence of Triton-X treated samples as 100 % release.

Nile red (NR) solubilisation assay. Prior to experiment, liposomes were prepared by mixing 50:50 of 1-palmitoyl-2-oleoyl-sn-glycero-3-phosphocholine (DMPC), and 1-palmitoyl-2-oleoyl-sn-glycero-3-phospho-(1'-rac-glycerol) (DMPG) in 20 mM, pH 7.5 phosphate buffer, followed by size exclusion with 200 nm membrane. Next, IAPP (12 μM) was mixed with different concentrations of 5 nm AuNPs (10.4, 5.2, 2.6, 0 nM) in 20 mM, pH 7.5 phosphate buffer for 10 min, before incubating the DMPC/DMPG liposomes with IAPP solution for 30 min. NR (10 μM) was added to the solution, and fluorescence spectra were collected after 1 h incubation at room temperature. The spectra were obtained by Perkin Elmer EnSpire plate reader, with an excitation wavelength of 575 nm, emission ranged from 590-750 nm, and data interval of 3 nm.

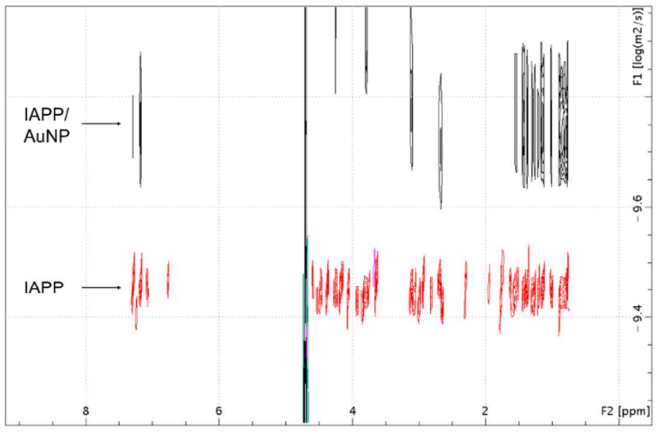

Figure S1 2D DOSY plot of diffusion data showing the observed differences in diffusion of IAPP monomer in the presence of AuNPs.

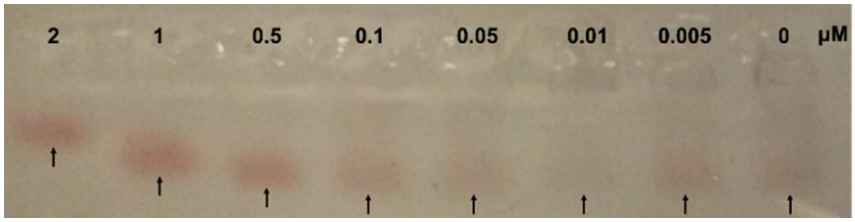

Figure S2 Agarose gel electrophoresis showing a reduced mobility of 5 nm AuNPs in the presence of different amounts of IAPP monomers, due to the binding of AuNPs to IAPP monomers.

Table S1 Summary of the surface charge of IAPP and AuNPs obtained by ζ-potential measurements. All the measurements were performed in phosphate buffer (20 mM, pH 7.5) and the values were averaged from triplicate measurements. The error was calculated by the standard error of the mean.

Sample	ζ-potential
IAPP monomer	7.3 ± 2.3
IAPP fibril	3.8 ± 0.8
2 nm AuNP	-23.8 ± 0.7
5 nm AuNP	-23.7 ± 4.4
10 nm AuNP	-21.9 ± 0.9
20 nm AuNP	-25.4 ± 4.4

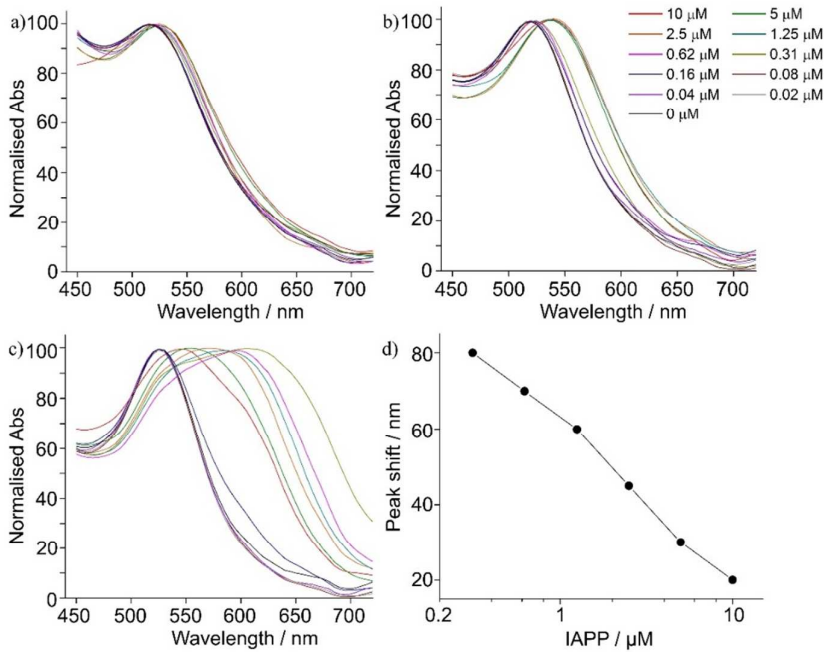

Figure S3 UV-vis spectra of AuNP solution: (a) 5 nm, (b) 10 nm, and (c) 20 nm in the presence of different concentrations of IAPP monomers. The aggregation was observed to be the strongest for 20 nm AuNPs. (d) Inverse plasmonic peak shifts were observed in the solution of 20 nm AuNPs and IAPP monomers (0.3 to 10 μM).

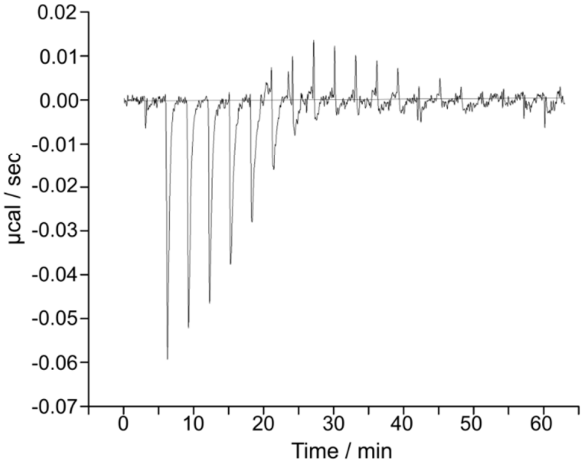

Figure S4 ITC thermogram of 120 µM IAPP 1-37 titrated to the solution of 5 nm AuNPs, showing the exothermic response. The thermal response from the corresponding control experiment has been subtracted from the measured data for the binding experiment.

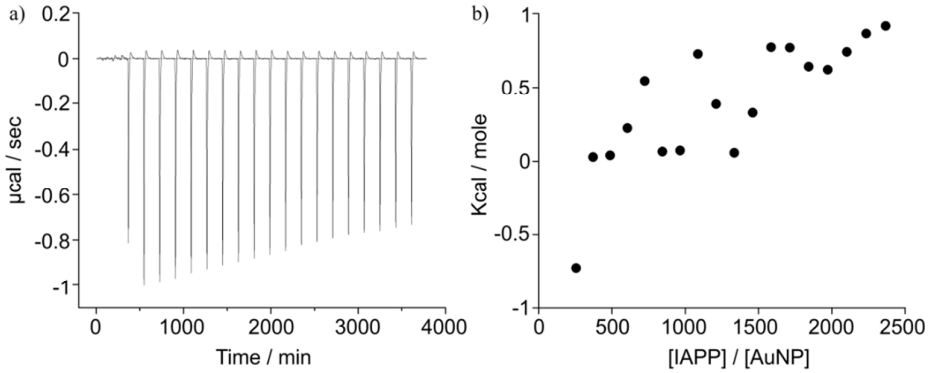

Figure S5 (a) ITC thermogram and (b) the integrated results of 120 µM IAPP 20-29 titrated to the solution of 5 nm AuNPs. The thermal response from the corresponding control experiment has been subtracted from the measured data in (a). The heat change was low and was not able to be processed by curve fitting to obtain the binding affinity and stoichiometry.

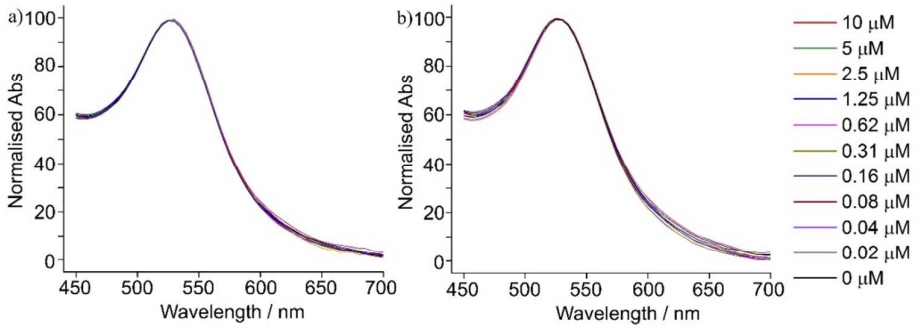

Figure S6 UV-vis spectra of 20 nm AuNPs in the presence of different concentrations of IAPP 20-29: (a) monomeric state and (b) fibrillar state, showing no aggregation of AuNPs was observed in both samples. The absorption spectra were measured in a 96-well plate, with a wavelength scan between 450 and 800 nm.

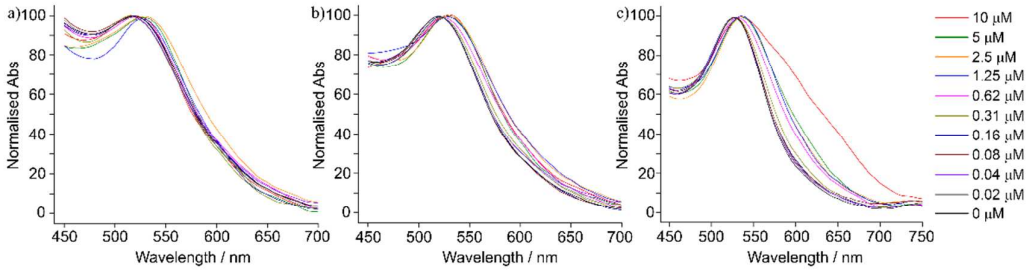

Figure S7 UV-vis spectra showing the aggregation of AuNPs in the presence of different concentrations of IAPP fibrils: (a) 5 nm, (b) 10 nm, and (c) 20 nm.

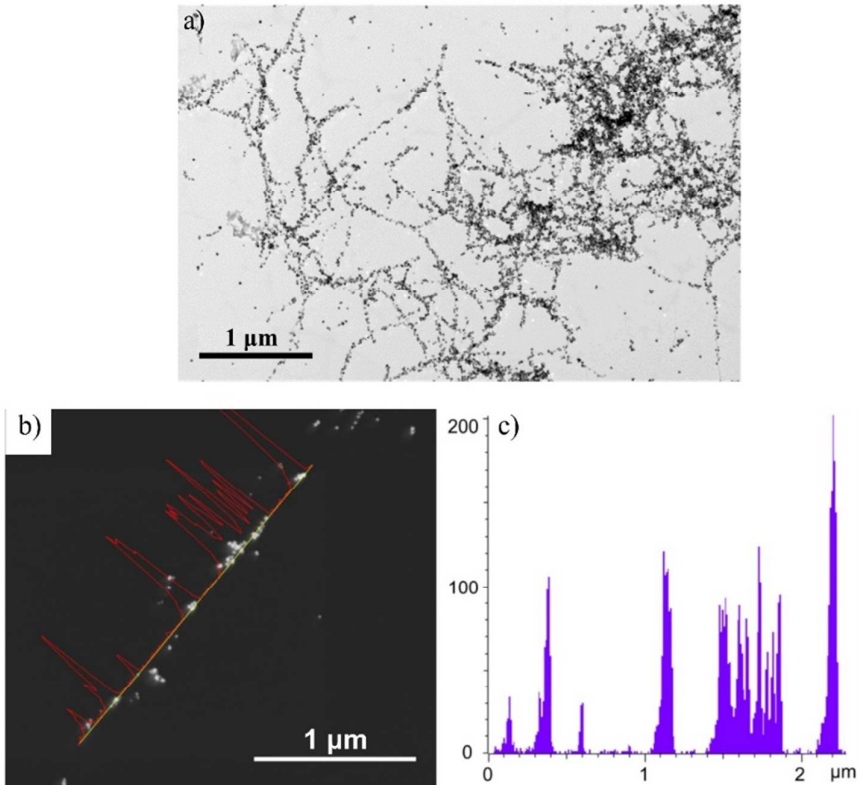

Figure S8 (a) TEM image and (b) dark field-scanning transmission electron microscopy (DF-STEM) image showing the direct growth of AuNPs on IAPP fibrils. (c) EDS was performed by line-scan over the fibril as shown in (b), in which the Au peaks matches the presence of AuNPs.

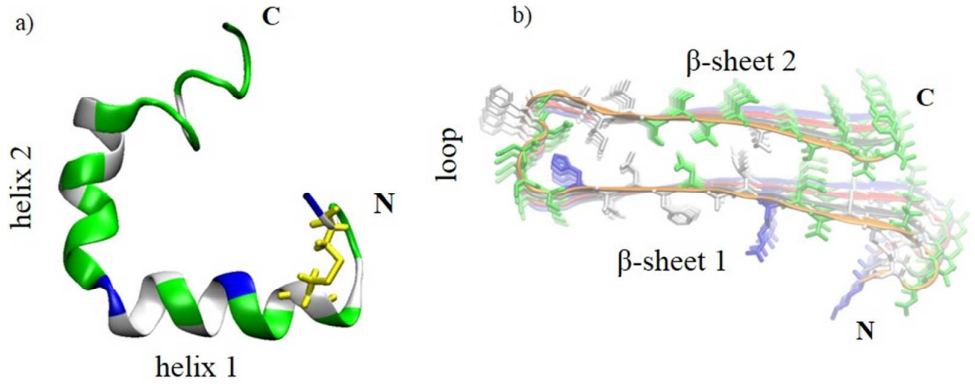

Figure S9 Starting structures of a) monomeric[9] and b) pre-formed fibril (tetramer)[11] IAPP used in the molecular dynamics simulations. The conformational domains are labelled as follows: *Monomer***:** N-ter (Res 1-5), Helix1 (Res 6-17), Helix2 (Res 19-28), C-ter (Res 29-37); *Fibril:* N-ter (Res 1-5), B-Sheet1 (Res 6-18), Loop (Res 19-24), B-Sheet2 (25-36), C-ter (Res 37).

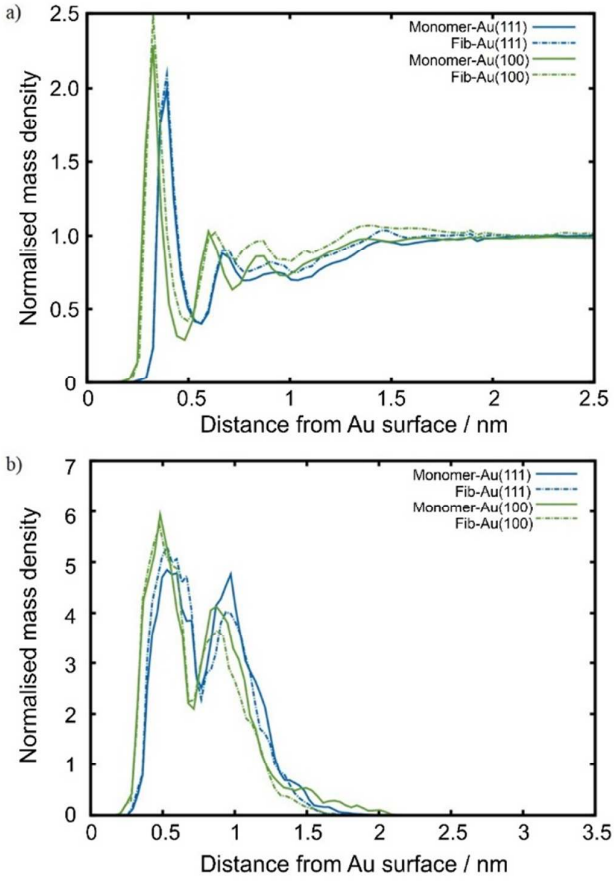

Figure S10 Representative mass density profiles of (a) water and (b) citrate molecules as a function of distance from the Au(111) (blue) and Au(100) (green) surfaces from the simulations of monomeric (solid line) and fibrillar (dashed line) IAPP.

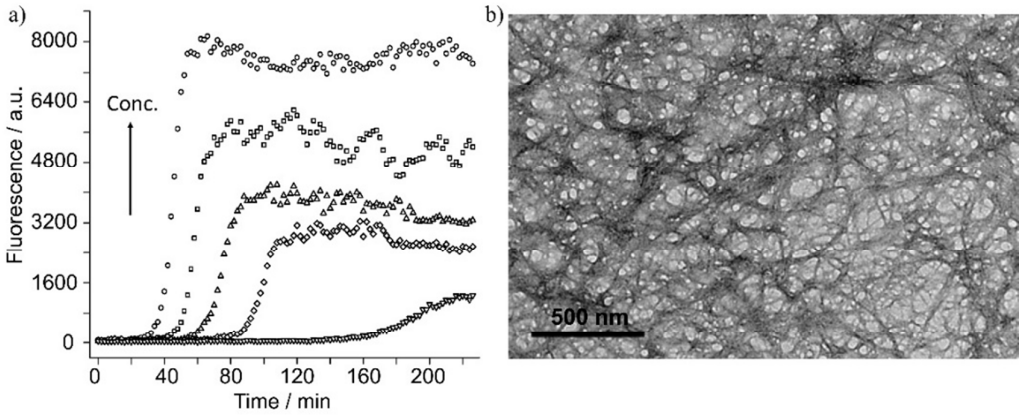

Figure S11 (a) Characterisation of IAPP fibrillation with ThT assay, showing the fibrillation kinetics was dependent on the peptide concentration (5, 10, 15, 20, 25 μM).

(b) TEM image showing the morphology of mature fibrils (25 μM) grown in solution. The fibrils were revealed by negative staining by 1 wt% uranyl acetate.

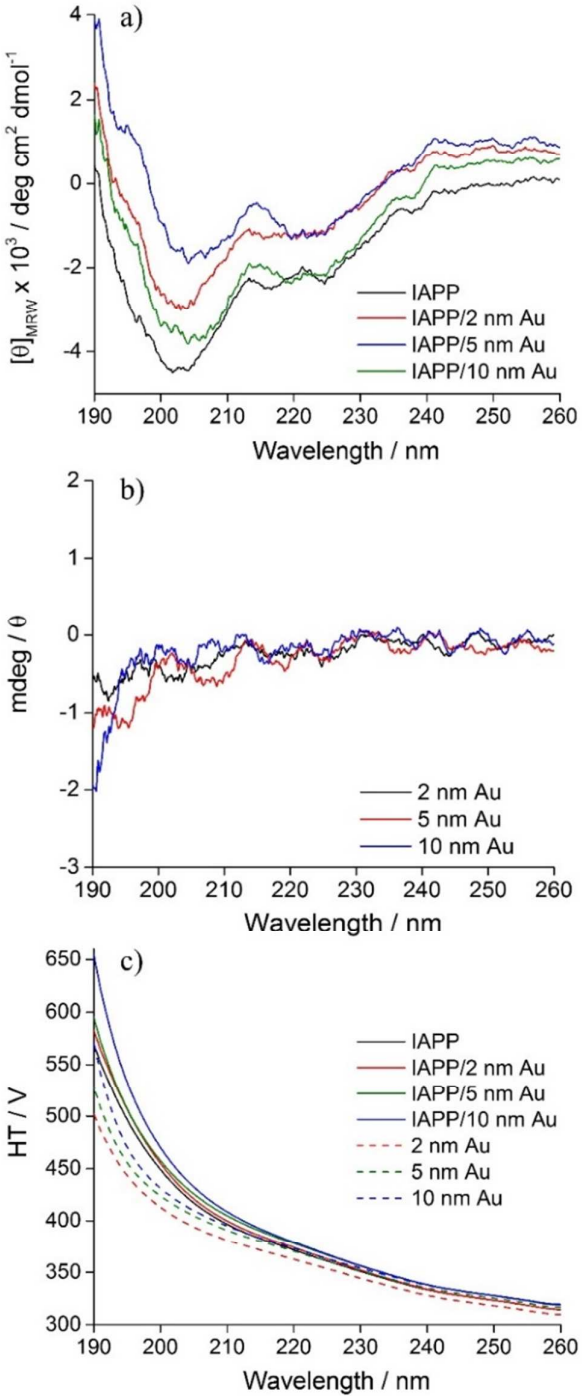

Figure S12 (a) CD spectra of IAPP (25 μM) in the absence and presence of 2 nm (20.8 nM), 5 nm (20.8 nM), and 10 nm (2.08 nM) AuNPs in single-scan measurements. The measurement was performed immediately after adding the

solution into the IAPP powder. (b) CD spectra of AuNPs in buffer solution in the absence of IAPP, and the (c) HT values of AuNPs in the presence and absence of IAPP. No noticeable absorbance was observed in the detecting wavelength (190-260 nm).

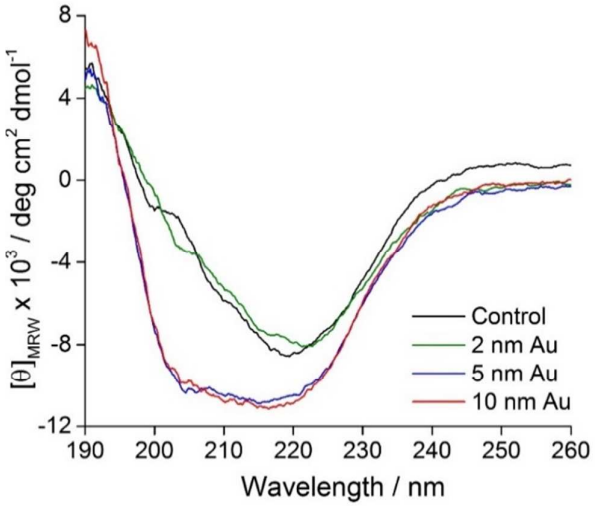

Figure S13 CD spectra of IAPP at 4 h in the absence and presence of 2 nm, 5 nm, and 10 nm AuNPs. The spectra were plotted from the kinetic measurements in Figure 4.

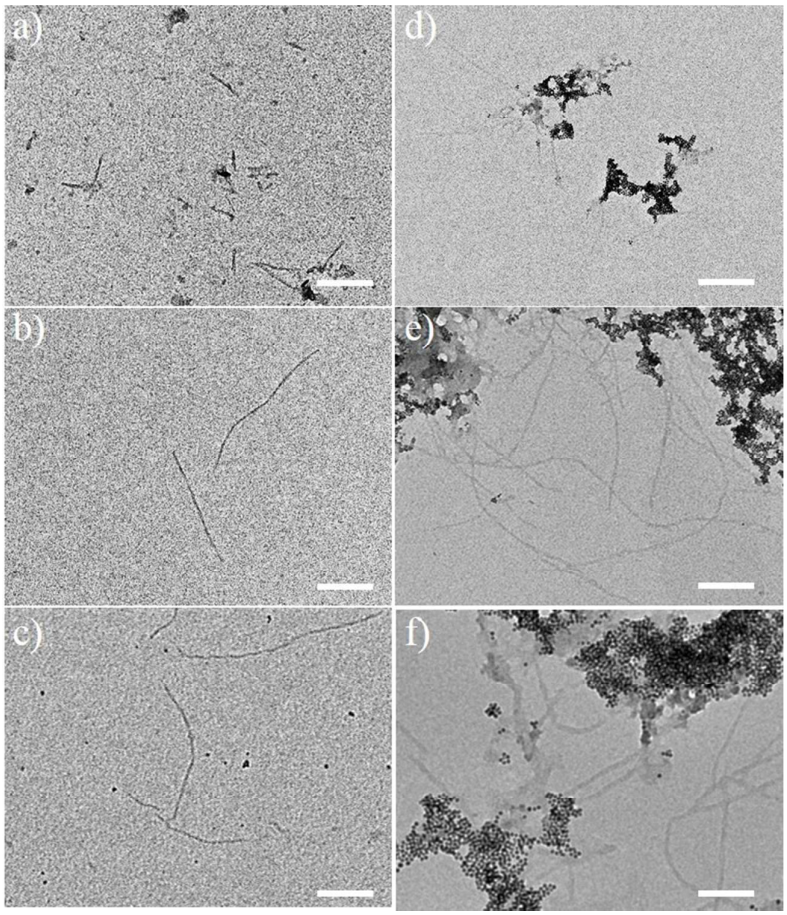

Figure S14 TEM images of IAPP (25 μM) fibrillation in the absence (a-c) and presence (d-f) of 5 nm AuNPs (20.8 nM) at shorter time points: (a, d) 10 min, (b, e) 30 min, and (c, f) 60 min, showing the fibrillation was accelerated by the presence of AuNPs. The samples were negatively stained with 1 wt% uranyl acetate. Scale bar: (a-e) 200 nm, (f) 100 nm.

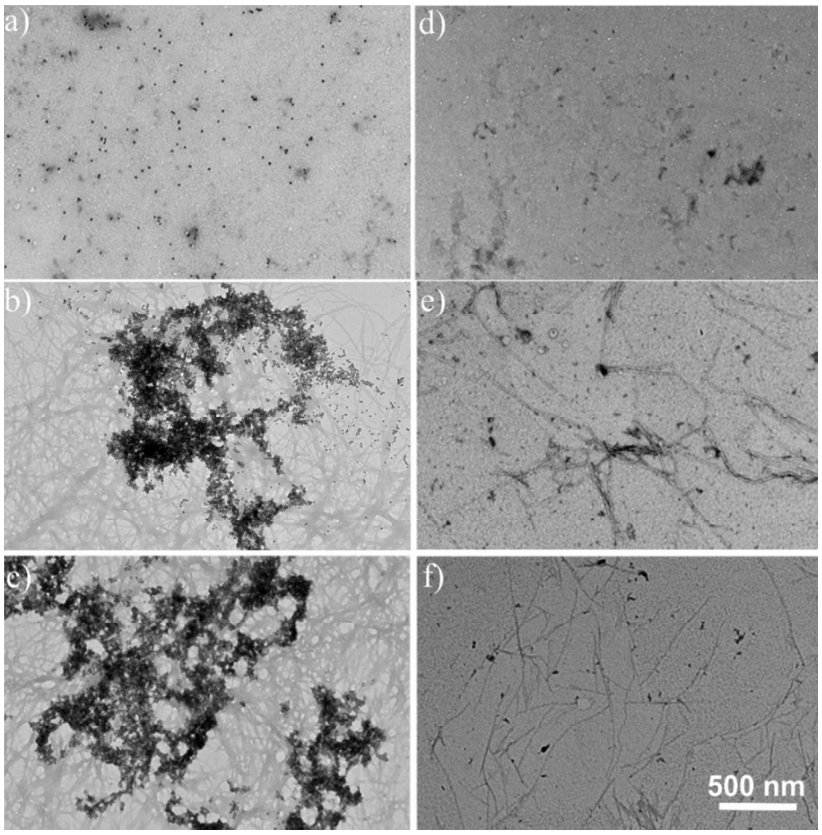

Figure S15 TEM images of IAPP (25 μM) fibrillation in the presence of (a-c) 10 nm AuNPs (2.08 nM), and (d-f) 2 nm AuNPs (20.8 nM). Images were taken at different time points: 0 h (a, d), 4 h (b, e), and 8 h (c, f).

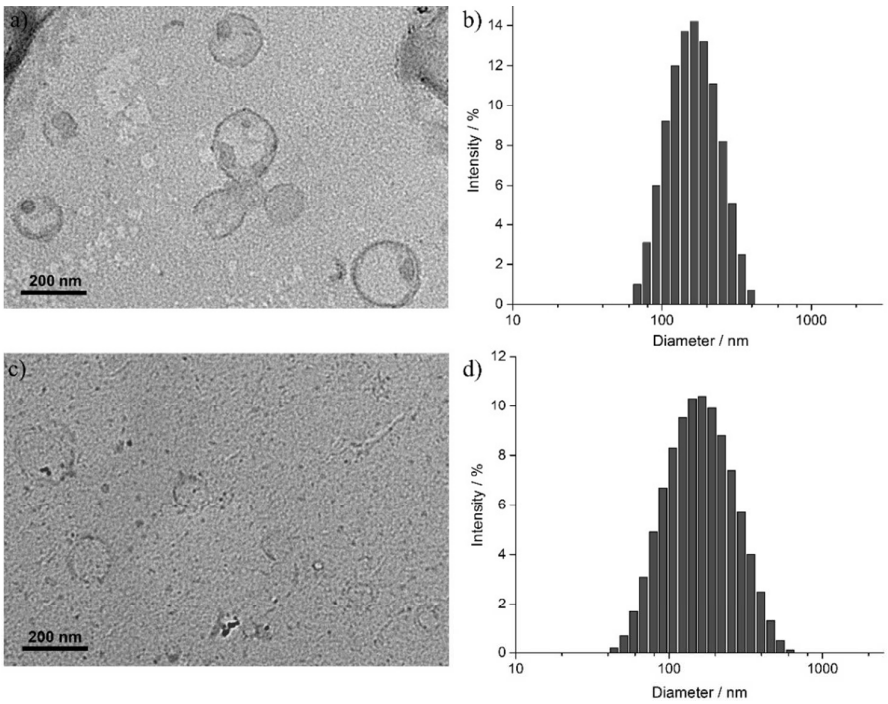

Figure S16 (a, c) TEM imaging and (b, d) dynamic light scattering (DLS) measurement showing the morphologies and sizes of (a, b) POPC/POPG (50:50), and (c, d) DMPC/DMPG (50:50) liposomes.

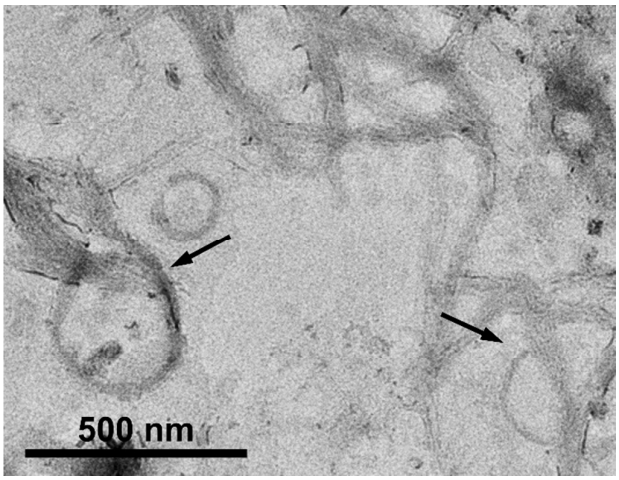

Figure S17 TEM image showing the interaction of IAPP with POPC/POPG (50:50) liposomes, which the peptide can penetrate through the lipid membranes during growth into larger fibrils (indicated by arrows).

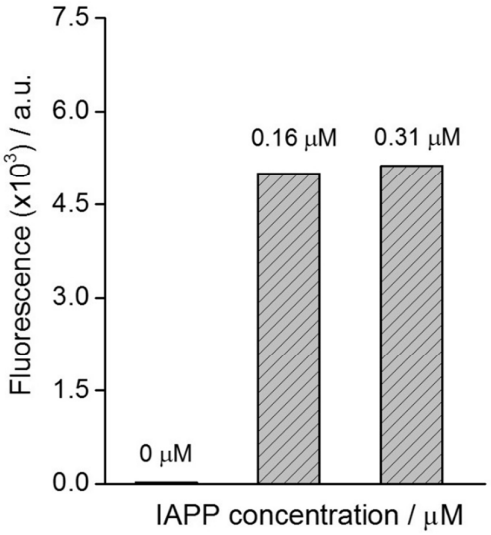

Figure S18 Dye leakage assay from CF-encapsulated POPC/POPG (50:50) liposomes triggered by IAPP oligomers. IAPP was dissolved in phosphate buffer (20 mM, pH 7.5) immediately before diluting into the liposome solutions. The fluorescence was recorded with an excitation of 485 nm and emission of 520 nm.

1. Stejskal, E. O.; Tanner, J. E., Spin Diffusion Measurements: Spin Echoes in the Presence of a Time-Dependent Field Gradient. *The Journal of Chemical Physics* **1965,** 42, (1), 288-292.
2. Salamekh, S.; Brender, J. R.; Hyung, S.-J.; Nanga, R. P. R.; Vivekanandan, S.; Ruotolo, B. T.; Ramamoorthy, A., A Two-Site Mechanism for the Inhibition of IAPP Amyloidogenesis by Zinc. *Journal of Molecular Biology* **2011,** 410, (2), 294-306.
3. Brender, J. R.; Krishnamoorthy, J.; Messina, G. M. L.; Deb, A.; Vivekanandan, S.; La Rosa, C.; Penner-Hahn, J. E.; Ramamoorthy, A., Zinc stabilization of prefibrillar oligomers of human islet amyloid polypeptide. *Chemical Communications* **2013,** 49, (32), 3339-3341.
4. Marks, L. D., Experimental studies of small particle structures. *Reports on Progress in Physics* **1994,** 57, (6), 603.
5. Brancolini, G.; Corazza, A.; Vuano, M.; Fogolari, F.; Mimmi, M. C.; Bellotti, V.; Stoppini, M.; Corni, S.; Esposito, G., Probing the Influence of Citrate-Capped Gold Nanoparticles on an Amyloidogenic Protein. *ACS Nano* **2015,** 9, (3), 2600-2613.
6. Lin, Y.; Pan, G.-B.; Su, G.-J.; Fang, X.-H.; Wan, L.-J.; Bai, C.-L., Study of Citrate Adsorbed on the Au(111) Surface by Scanning Probe Microscopy. *Langmuir* **2003,** 19, (24), 10000-10003.
7. Rostek, A.; Mahl, D.; Epple, M., Chemical composition of surface-functionalized gold nanoparticles. *Journal of Nanoparticle Research* **2011,** 13, (10), 4809-4814.
8. Wright, L. B.; Rodger, P. M.; Walsh, T. R., Structure and Properties of Citrate Overlayers Adsorbed at the Aqueous Au(111) Interface. *Langmuir* **2014,** 30, (50), 15171-15180.
9. Nanga, R. P.; Brender, J. R.; Vivekanandan, S.; Ramamoorthy, A., Structure and membrane orientation of IAPP in its natively amidated form at physiological pH in a membrane environment. *Biochim Biophys Acta* **2011,** 1808, (10), 2337-42.
10. Wiltzius, J. J. W.; Sievers, S. A.; Sawaya, M. R.; Cascio, D.; Popov, D.; Riekel, C.; Eisenberg, D., Atomic structure of the cross-β spine of islet amyloid polypeptide (amylin). *Protein Science* **2008,** 17, (9), 1467-1474.
11. Smaoui, Mohamed R.; Poitevin, F.; Delarue, M.; Koehl, P.; Orland, H.; Waldispühl, J., Computational Assembly of Polymorphic Amyloid Fibrils Reveals Stable Aggregates. *Biophysical Journal* **2013,** 104, (3), 683-693.
12. Berendsen, H. J. C.; van der Spoel, D.; van Drunen, R., GROMACS: A message-passing parallel molecular dynamics implementation. *Computer Physics Communications* **1995,** 91, (1–3), 43-56.
13. Wright, L. B.; Rodger, P. M.; Corni, S.; Walsh, T. R., GolP-CHARMM: First-Principles Based Force Fields for the Interaction of Proteins with Au(111) and Au(100). *Journal of Chemical Theory and Computation* **2013,** 9, (3), 1616-1630.
14. Wright, L. B.; Rodger, P. M.; Walsh, T. R., Aqueous citrate: a first-principles and force-field molecular dynamics study. *RSC Advances* **2013,** 3, (37), 16399-16409.
15. Jorgensen, W. L.; Chandrasekhar, J.; Madura, J. D.; Impey, R. W.; Klein, M. L., Comparison of simple potential functions for simulating liquid water. *The Journal of Chemical Physics* **1983,** 79, (2), 926-935.
16. Iori, F.; Di Felice, R.; Molinari, E.; Corni, S., GolP: an atomistic force-field to describe the interaction of proteins with Au(111) surfaces in water. *J Comput Chem* **2009,** 30, (9), 1465-76.
17. Barone, V.; Casarin, M.; Forrer, D.; Monti, S.; Prampolini, G., Molecular Dynamics Simulations of the Self-Assembly of Tetraphenylporphyrin-Based Monolayers and Bilayers at a Silver Interface. *The Journal of Physical Chemistry C* **2011,** 115, (38), 18434-18444.
18. Mendonça, A. C. F.; Malfreyt, P.; Pádua, A. A. H., Interactions and Ordering of Ionic Liquids at a Metal Surface. *Journal of Chemical Theory and Computation* **2012,** 8, (9), 3348-3355.
19. Hakkinen, H., The gold-sulfur interface at the nanoscale. *Nat Chem* **2012,** 4, (6), 443-455.
20. Darden, T.; York, D.; Pedersen, L., Particle mesh Ewald: An N·log(N) method for Ewald sums in large systems. *The Journal of Chemical Physics* **1993,** 98, (12), 10089-10092.

21. Nosé, S., A molecular dynamics method for simulations in the canonical ensemble. *Molecular Physics* **1984,** 52, (2), 255-268.
22. Hess, B.; Bekker, H.; Berendsen, H. J. C.; Fraaije, J. G. E. M., LINCS: A linear constraint solver for molecular simulations. *Journal of Computational Chemistry* **1997,** 18, (12), 1463-1472.
23. Humphrey, W.; Dalke, A.; Schulten, K., VMD: visual molecular dynamics. *Journal of molecular graphics* **1996,** 14, (1), 33-8, 27-8.